IOPscience iopscience.iop.org

Home Search Collections Journals About Contact us My IOPscience

An efficient hybrid pseudospectral/finite-difference scheme for solving the TTI pure P-wave equation

This article has been downloaded from IOPscience. Please scroll down to see the full text article.

2013 J. Geophys. Eng. 10 025004

(http://iopscience.iop.org/1742-2140/10/2/025004)

View the table of contents for this issue, or go to the journal homepage for more

Download details:
IP Address: 200.130.19.138
The article was downloaded on 17/06/2013 at 13:58

Please note that terms and conditions apply.

IOP Publishing Journal of Geophysics and Engineering

J. Geophys. Eng. **10** (2013) 025004 (8pp) doi:10.1088/1742-2132/10/2/025004

An efficient hybrid pseudospectral/finite-difference scheme for solving the TTI pure P-wave equation

Ge Zhan[1], **Reynam C Pestana**[2] **and Paul L Stoffa**[3]

[1] Earth Science and Engineering, King Abdullah University of Science and Technology (KAUST), Thuwal 23955-6900, Saudi Arabia
[2] Geophysics, Federal University of Bahia (UFBA), Rua Barao de Geremoabo, Salvador, Bahia 40110-060, Brazil
[3] Institute for Geophysics, University of Texas at Austin, Austin, TX 78713-8924, USA

E-mail: ge.zhan@kaust.edu.sa

Received 27 September 2012
Accepted for publication 22 January 2013
Published 18 February 2013
Online at stacks.iop.org/JGE/10/025004

Abstract
The pure P-wave equation for modelling and migration in tilted transversely isotropic (TTI) media has attracted more and more attention in imaging seismic data with anisotropy. The desirable feature is that it is absolutely free of shear-wave artefacts and the consequent alleviation of numerical instabilities generally suffered by some systems of coupled equations. However, due to several forward–backward Fourier transforms in wavefield updating at each time step, the computational cost is significant, and thereby hampers its prevalence. We propose to use a hybrid pseudospectral (PS) and finite-difference (FD) scheme to solve the pure P-wave equation. In the hybrid solution, most of the cost-consuming wavenumber terms in the equation are replaced by inexpensive FD operators, which in turn accelerates the computation and reduces the computational cost. To demonstrate the benefit in cost saving of the new scheme, 2D and 3D reverse-time migration (RTM) examples using the hybrid solution to the pure P-wave equation are carried out, and respective runtimes are listed and compared. Numerical results show that the hybrid strategy demands less computation time and is faster than using the PS method alone. Furthermore, this new TTI RTM algorithm with the hybrid method is computationally less expensive than that with the FD solution to conventional TTI coupled equations.

Keywords: TTI wave equation, hybrid solution

(Some figures may appear in colour only in the online journal)

1. Introduction

Various methods for modelling anisotropic acoustic seismic waves (Alkhalifah 1998, Zhou *et al* 2006a, Du *et al* 2008) as well as wavefronts and rays (Bos and Slawinski 2010, Epstein *et al* 2012) have been proposed and developed, especially for vertical transversely isotropic (VTI) and tilted transversely isotropic (TTI) media. In general, we can divide those methods into two broad categories: methods that suffered from shear-wave artefacts, usually known as coupled equations where P and shear waves are coupled together (Alkhalifah 2000, Zhou *et al* 2006a, 2006b, Fletcher *et al* 2009, Fowler *et al* 2010, Duveneck and Bakker 2011), and pure P-wave (or decoupled) equations which are free of shear-wave artefacts (Etgen and Brandsberg-Dahl 2009, Liu *et al* 2009, Chu *et al* 2011, Pestana *et al* 2012, Zhan *et al* 2012). Each has its pros and cons as summarized in table 1.

The pure P-wave equation in the system of decoupled equations of Zhan *et al* (2012) is in the wavenumber domain, and at each time step it requires 8 fast Fourier transforms (FFTs) for 2D and 22 FFTs for 3D. This imposes an unrealistic demand for practical migration of large-scale 3D field seismic data sets. In the work presented below, we follow the same

 © 2013 Sinopec Geophysical Research Institute Printed in the UK

Table 1. Computational characteristics of TTI coupled equations versus decoupled equations.

Category	Number of equations to solve	Method of solution	Shear-wave artefacts	Numerical stability with variable angles	Cost
Coupled equations	2	FD	Yes	Unstable	Efficient
		PS	No	Unstable	Intensive
Pure P-wave equation	1	PS	No	More stable	Intensive

derivations as Pestana *et al* (2012) and Zhan *et al* (2012), but reorganize and rewrite the wavenumber domain equation in a compact way for efficient computation. After some algebraic manipulations, it still requires 8 FFTs per time step for 2D computation with the new formulation, but the number of FFTs needed per time step for 3D is reduced from 22 to 14.

To further reduce the computational cost introduced by numerous FFTs, we propose a hybrid pseudo-spectral (PS) and finite-difference (FD) scheme to evaluate the equation by using the relation between the spatial derivative and the operator in the wavenumber domain. Both 2D and 3D reverse-time migration (RTM) examples with the new hybrid algorithm are tested and demonstrated to validate the uplift in computational efficiency.

2. Equations

2.1. Isotropic wave equation

The constant-density acoustic wave equation in isotropic media is

$$\frac{\partial^2 u(\vec{x},t)}{\partial t^2} = L^2 u(\vec{x},t), \tag{1}$$

where $u(\vec{x},t)$ is the pressure wavefield at spatial location $\vec{x} = (x,y,z)$ and time t; $L^2 = v^2(\vec{x})\nabla^2$, where $v(\vec{x})$ is the P-wave velocity in the medium and ∇^2 is the Laplacian defined as $\nabla^2 = \partial_x^2 + \partial_y^2 + \partial_z^2$. An efficient numerical solution of the wave equation on a discrete grid is our main interest. To solve the discretized version of equation (1), we approximate the temporal (left) and spatial (right) derivatives in the equation, where the time derivative is approximated by a second-order FD approximation

$$u(\vec{x},t+\Delta t) = 2u(\vec{x},t) - u(\vec{x},t-\Delta t) - \Delta t^2[-L^2 u(\vec{x},t)]. \tag{2}$$

Here, Δt denotes the length of a discrete time step.

The PS method (Reshef *et al* 1988) is known as a highly accurate scheme for approximating the Laplacian operator. In doing so, the numerical errors in the solution of the wave equation are only dominated by the temporal discretization. For the isotropic case, the $-L^2$ operator in equation (2) can be expressed in the wavenumber domain

$$-L^2 = v_v^2\left(k_x^2 + k_y^2 + k_z^2\right) = v_v^2\left(k_r^2 + k_z^2\right) = v_v^2 k_\rho^2, \tag{3}$$

where v_v is the velocity of a wave travelling vertically along the axis of symmetry; k_x, k_y and k_z are the spatial wavenumbers in the x, y and z directions, respectively; $k_r^2 = k_x^2 + k_y^2$ and $k_\rho^2 = k_x^2 + k_y^2 + k_z^2$.

2.2. VTI pure P-wave equation

In the case of VTI, based on Harlan (1995) and later rediscovered by Etgen and Brandsberg-Dahl (2009), Crawley *et al* (2010), Pestana *et al* (2012) and Zhan *et al* (2012) where they started from the exact phase velocity expression for VTI media, equation (3) becomes

$$-L^2 = v_v^2 k_z^2 + v_h^2 k_r^2 + \left(v_n^2 - v_h^2\right)\frac{k_r^2 k_z^2}{k_\rho^2}. \tag{4}$$

Here, $v_n = v_v\sqrt{1+2\delta}$ and $v_h = v_v\sqrt{1+2\varepsilon}$ represent the normal moveout (NMO) velocity and the P-wave velocity in the horizontal direction, respectively; δ and ε are the anisotropy parameters (Thomsen 1986).

The resulting anisotropic wave equation derived in this way is known as the pure P-wave or decoupled equation, where the P-wave and shear-wave components are completely separated and there are no spurious shear-wave artefacts in the P-wave simulation.

2.3. TTI pure P-wave equation

A similar expression for TTI media can be deduced from equation (4) through variable exchanges (Zhan *et al* 2012)

$$-L^2 = v_v^2 k_{\tilde{z}}^2 + v_h^2 k_{\tilde{r}}^2 + \left(v_n^2 - v_h^2\right)\frac{k_{\tilde{r}}^2 k_{\tilde{z}}^2}{k_\rho^2}, \tag{5}$$

where $k_{\tilde{r}}^2 = k_{\tilde{x}}^2 + k_{\tilde{y}}^2$ with $k_{\tilde{x}}$, $k_{\tilde{y}}$ and $k_{\tilde{z}}$ representing the spatial wavenumbers in the rotated coordinate system

$$\begin{bmatrix} k_{\tilde{x}} \\ k_{\tilde{y}} \\ k_{\tilde{z}} \end{bmatrix} = \begin{bmatrix} \cos\theta\cos\phi & \cos\theta\sin\phi & \sin\theta \\ -\sin\phi & \cos\phi & 0 \\ -\sin\theta\cos\phi & -\sin\theta\sin\phi & \cos\theta \end{bmatrix} \begin{bmatrix} k_x \\ k_y \\ k_z \end{bmatrix}. \tag{6}$$

Here θ and ϕ are dip and azimuth, and the following relation holds:

$$k_{\tilde{x}}^2 + k_{\tilde{y}}^2 + k_{\tilde{z}}^2 = k_x^2 + k_y^2 + k_z^2. \tag{7}$$

In the case of elliptical anisotropy where $\varepsilon = \delta$ (i.e. $v_h = v_n$), the last term of equation (5) with wavenumbers in the denominator disappears. Therefore, the first two terms in equation (5) represent the properties of elliptical anisotropy, while the last term compensates for anelliptical anisotropic effects due to the rotation of the symmetry axis.

According to the rotation matrix (6), and denoting $\Gamma_x = \sin\theta\cos\phi$, $\Gamma_y = \sin\theta\sin\phi$ and $\Gamma_z = -\cos\theta$, we can rewrite $k_{\tilde{z}}$ in the rotated system in terms of k_x, k_y and k_z:

$$\begin{aligned} k_{\tilde{z}} &= -(k_x\sin\theta\cos\phi + k_y\sin\theta\sin\phi - k_z\cos\theta) \\ &= -(k_x\Gamma_x + k_y\Gamma_y + k_z\Gamma_z). \end{aligned} \tag{8}$$

Hence, the three wavenumber terms in equation (5) can be computed in the following order:

$$k_z^2 = k_x^2\Gamma_{xx} + k_y^2\Gamma_{yy} + k_z^2\Gamma_{zz} + 2(k_xk_y\Gamma_{xy} + k_yk_z\Gamma_{yz} + k_xk_z\Gamma_{xz}) = V, \tag{9a}$$

$$k_r^2 = k_\rho^2 - V = H, \tag{9b}$$

$$\frac{k_r^2k_z^2}{k_\rho^2} = \left[\frac{k_x^2}{k_\rho^2}\Gamma_{xx} + \frac{k_y^2}{k_\rho^2}\Gamma_{yy} + \frac{k_z^2}{k_\rho^2}\Gamma_{zz} + 2\left(\frac{k_xk_y}{k_\rho^2}\Gamma_{xy} + \frac{k_yk_z}{k_\rho^2}\Gamma_{yz} + \frac{k_xk_z}{k_\rho^2}\Gamma_{xz}\right)\right]H = T, \tag{9c}$$

where $\Gamma_{ij} = \Gamma_i\Gamma_j$; V, H and T are differential operators in the wavenumber domain that operate along the symmetry axis direction, the symmetry plane perpendicular to the symmetry axis and the tilted direction, respectively.

3. Numerical implementations

3.1. Pseudospectral scheme

The PS method is proposed by Kosloff and Baysal (1982), which uses Fourier transformation, multiplication by ik in the wavenumber domain and inverse Fourier transformation back to the spatial domain to compute the spatial derivatives. Differential operators V, H and T in equation (9) are written in the wavenumber domain and are easily evaluated there with the PS method. Meanwhile, as in the PS method, performing the operations in the wavenumber domain guarantees that it will not suffer from numerical dispersion.

Substituting equations (5) and (9) into equation (2), we write the TTI pure P-wave equation as

$$\begin{aligned} u(\vec{x},t+\Delta t) &= 2u(\vec{x},t) - u(\vec{x},t-\Delta t) \\ &\quad - \Delta t^2\left\{\left[v_v^2V + v_h^2H + (v_n^2 - v_h^2)T\right]u(\vec{x},t)\right\} \\ &= 2u(\vec{x},t) - u(\vec{x},t-\Delta t) - \Delta t^2\left\{v_v^2\mathcal{F}^{-1}[V\mathcal{F}[u(\vec{x},t)]]\right. \\ &\quad \left. + v_h^2\mathcal{F}^{-1}[H\mathcal{F}[u(\vec{x},t)]] + (v_n^2 - v_h^2)\mathcal{F}^{-1}[T\mathcal{F}[u(\vec{x},t)]]\right\}, \end{aligned} \tag{10}$$

where $\mathcal{F}$ and $\mathcal{F}^{-1}$ are forward and inverse FFTs, respectively.

From the above equations, we can see that at each time step of a 3D simulation, the evaluation of the differential operator V demands at least a 3D forward FFT of the wavefield plus six 3D inverse FFTs. A similar analysis applies to the differential operator T as well. Therefore, a total of 14 3D FFTs are required to simulate the pure P-wave wavefield at each time step in a TTI medium. When it comes to 2D, all k_y terms are eliminated, and thus only eight 2D FFTs are needed.

3.2. Hybrid pseudospectral/finite-difference scheme

During each time step, the TTI pure P-wave computation in equation (10) requires 2 forward FFTs and 12 inverse FFTs, which is computationally intensive. By revisiting equation (9), we find that due to the appearance of the wavenumbers in the denominators, equation (9c) must be evaluated using the PS method and it would be difficult to derive pure FD operators that correspond to the six right-hand-side terms. However, there are no such terms in equations (9a) and (9b). To greatly reduce the computation cost while avoiding spurious shear-wave artefacts as well as numerical instabilities, we propose a hybrid PS/FD scheme to evaluate the TTI pure P-wave equation given in equation (10). That is, transforming equations (9a) and (9b) using the relations $k_x \leftrightarrow -\mathrm{i}\frac{\partial}{\partial x}$, $k_y \leftrightarrow -\mathrm{i}\frac{\partial}{\partial y}$, $k_z \leftrightarrow -\mathrm{i}\frac{\partial}{\partial z}$ yields

$$k_z^2 \leftrightarrow -\left[\frac{\partial^2}{\partial x^2}\Gamma_{xx} + \frac{\partial^2}{\partial y^2}\Gamma_{yy} + \frac{\partial^2}{\partial z^2}\Gamma_{zz} + 2\left(\frac{\partial^2}{\partial x\partial y}\Gamma_{xy} + \frac{\partial^2}{\partial y\partial z}\Gamma_{yz} + \frac{\partial^2}{\partial x\partial z}\Gamma_{xz}\right)\right] = V', \tag{11a}$$

$$k_r^2 \leftrightarrow -\left(\frac{\partial^2}{\partial x^2} + \frac{\partial^2}{\partial y^2} + \frac{\partial^2}{\partial z^2}\right) - V' = H', \tag{11b}$$

where V' and H' can be approximated by FD operators applied along the symmetry axis and symmetry plane, respectively. Spatial derivatives in the above equation can be cheaply computed using a second-, fourth- or higher-order FD scheme instead of using FFTs back and forth.

Although the wavenumber terms in equation (9c) cannot all be replaced by corresponding FD operators, they could be partially approximated as follows:

$$\begin{aligned} \frac{k_r^2k_z^2}{k_\rho^2} &= \left[k_x\frac{k_x}{k_\rho^2}\Gamma_{xx} + k_y\frac{k_y}{k_\rho^2}\Gamma_{yy} + k_z\frac{k_z}{k_\rho^2}\Gamma_{zz} + 2\left(k_y\frac{k_x}{k_\rho^2}\Gamma_{xy} + k_z\frac{k_y}{k_\rho^2}\Gamma_{yz} + k_x\frac{k_z}{k_\rho^2}\Gamma_{xz}\right)\right]H \\ &= \left[(k_x\Gamma_{xx} + 2k_y\Gamma_{xy})\frac{k_x}{k_\rho^2} + (k_y\Gamma_{yy} + 2k_z\Gamma_{yz})\frac{k_y}{k_\rho^2} + (k_z\Gamma_{zz} + 2k_x\Gamma_{xz})\frac{k_z}{k_\rho^2}\right]H \\ &\leftrightarrow \left[\left(\frac{\partial}{\partial x}\Gamma_{xx} + 2\frac{\partial}{\partial y}\Gamma_{xy}\right)\frac{-\mathrm{i}k_x}{k_\rho^2} + \left(\frac{\partial}{\partial y}\Gamma_{yy} + 2\frac{\partial}{\partial z}\Gamma_{yz}\right)\times\frac{-\mathrm{i}k_y}{k_\rho^2} + \left(\frac{\partial}{\partial z}\Gamma_{zz} + 2\frac{\partial}{\partial x}\Gamma_{xz}\right)\frac{-\mathrm{i}k_z}{k_\rho^2}\right]H \\ &= T'. \end{aligned} \tag{11c}$$

Note that the number of wavenumber terms in equation (11c) is reduced from six to three. And T' can now be approximated by FD operators as well as V' and H'.

Therefore, the resulting hybrid solution to the TTI pure P-wave equation becomes

$$u(\vec{x},t+\Delta t) = 2u(\vec{x},t) - u(\vec{x},t-\Delta t) - \Delta t^2\left[v_v^2V' + v_h^2H' + \left(v_n^2 - v_h^2\right)T'\right]u(\vec{x},t). \tag{12}$$

Notably, the proposed hybrid strategy only requires four (one forward and three inverse) 3D FFTs per time step in simulating a pure P-wave propagation in a 3D TTI medium. For a 2D model, the number of FFTs reduces to three per time step with the hybrid method.

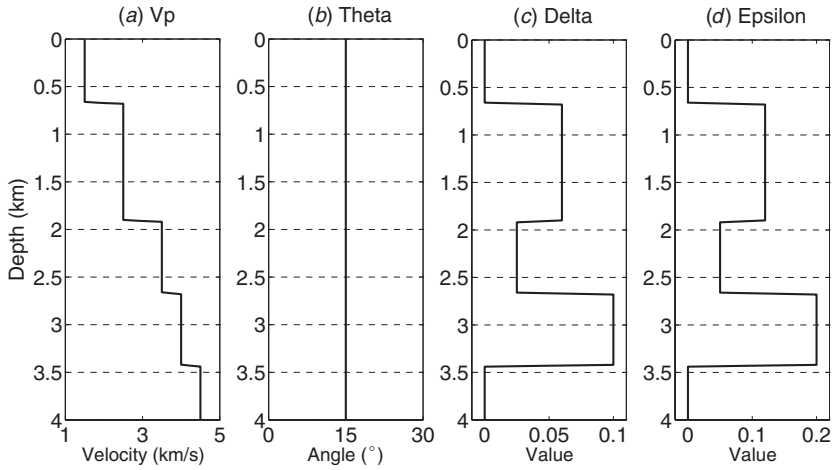

Figure 1. Anisotropic model parameters used in the accuracy test.

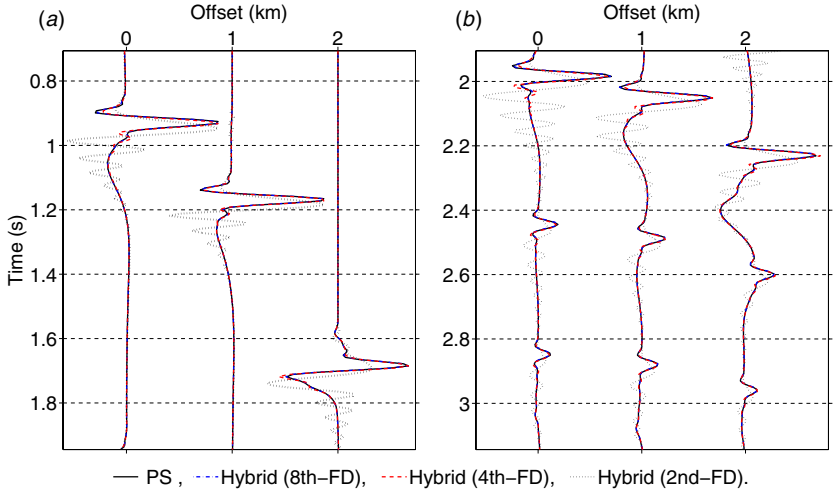

Figure 2. Three traces computed from the 2D five-layer TTI model are displayed in wiggle mode. (*a*) compares the first (strongest) reflection event, while (*b*) compares lower (weak) reflections.

Table 2. Number of FFTs per time step in simulating the TTI wavefield: pseudospectral scheme versus hybrid scheme.

	Dimension	
Method	2D	3D
PS	8	14
Hybrid	3	4

3.3. Comparison of the two schemes

The most computationally intensive parts in solving the TTI pure P-wave equation are the FFT calculations; therefore, we need to count and compare the total number of FFTs in each scheme. Table 2 displays the number of FFTs in modelling the TTI wavefield at a time step with the pure P-wave equation by the standard PS scheme and the new hybrid scheme. Obviously, the number of FFTs using the hybrid method is reduced by more than half in comparison with that using the PS method, which indicates that the hybrid algorithm is more computationally efficient compared to the standard PS scheme. Nevertheless, the disadvantage of the hybrid scheme is that it is no longer as accurate as the standard PS scheme.

3.4. Accuracy comparison

For the proposed hybrid PS/FD method, the costs of derivative calculations are reduced at the expense of the precision, as well as the accuracy of the solution, because some of the wavenumber operators are substituted by FD approximations. To demonstrate the consequent accuracy loss, we conduct a 2D modelling test on a simple five-layer TTI model. Figure 1 displays the model parameters that are used in this test. The spatial interval of the computational grid is 10 m, and the maximum frequency of the source wavelet is 30 Hz.

First, equation (10) using the standard PS method is implemented. Then, equation (12) using the hybrid method is computed, where the spatial derivatives in equations (11*a*), (11*b*) and (11*c*) are approximated and calculated using second-, fourth- and eighth-order centred FD schemes from Taylor series expansions, respectively. To check the amplitude differences, three wiggle traces at zero/middle/far offsets computed using different methods are plotted and

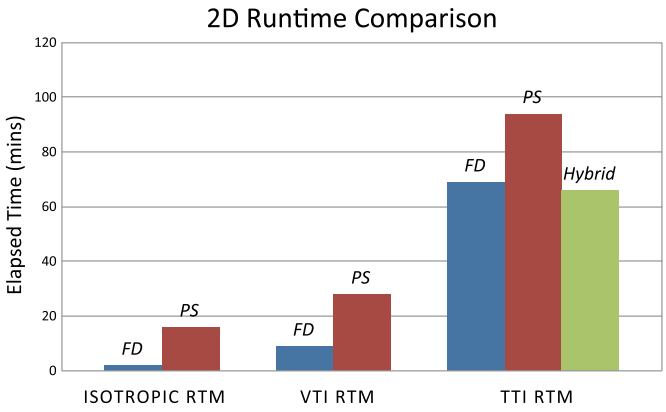

Figure 3. Histogram comparison of the 2D RTM runtimes.

compared in figure 2. As we can see from figure 2, amplitudes computed from the PS method and the hybrid method with the eighth-order FD scheme are perfectly matched. And the computational costs of these two methods are almost equivalent. When the fourth-order FD scheme is used, all major amplitudes from shallow to deep are still well matched to the PS result, except that some tiny discrepancies start to appear due to numerical dispersion. However, the runtime is reduced by half. A more compact second-order FD scheme may further improve the computational efficiency; however, both the amplitude discrepancies and phase errors are maximized due to the strong dispersive behaviour associated with smaller stencils.

According to the above analysis, in latter numerical examples, the fourth-order FD scheme is chosen to compute spatial derivatives in the hybrid method in terms of accuracy and efficiency.

4. Computation examples

Computation examples associated with the BP 2D TTI model as well as a 3D salt dome model are now presented to validate the proposed hybrid PS/FD scheme. TTI RTM algorithms with the pure P-wave equation using both the PS method and the hybrid method are implemented. Computational costs of running single common-shot-gather (CSG) migration with different approaches are demonstrated. For comparison,

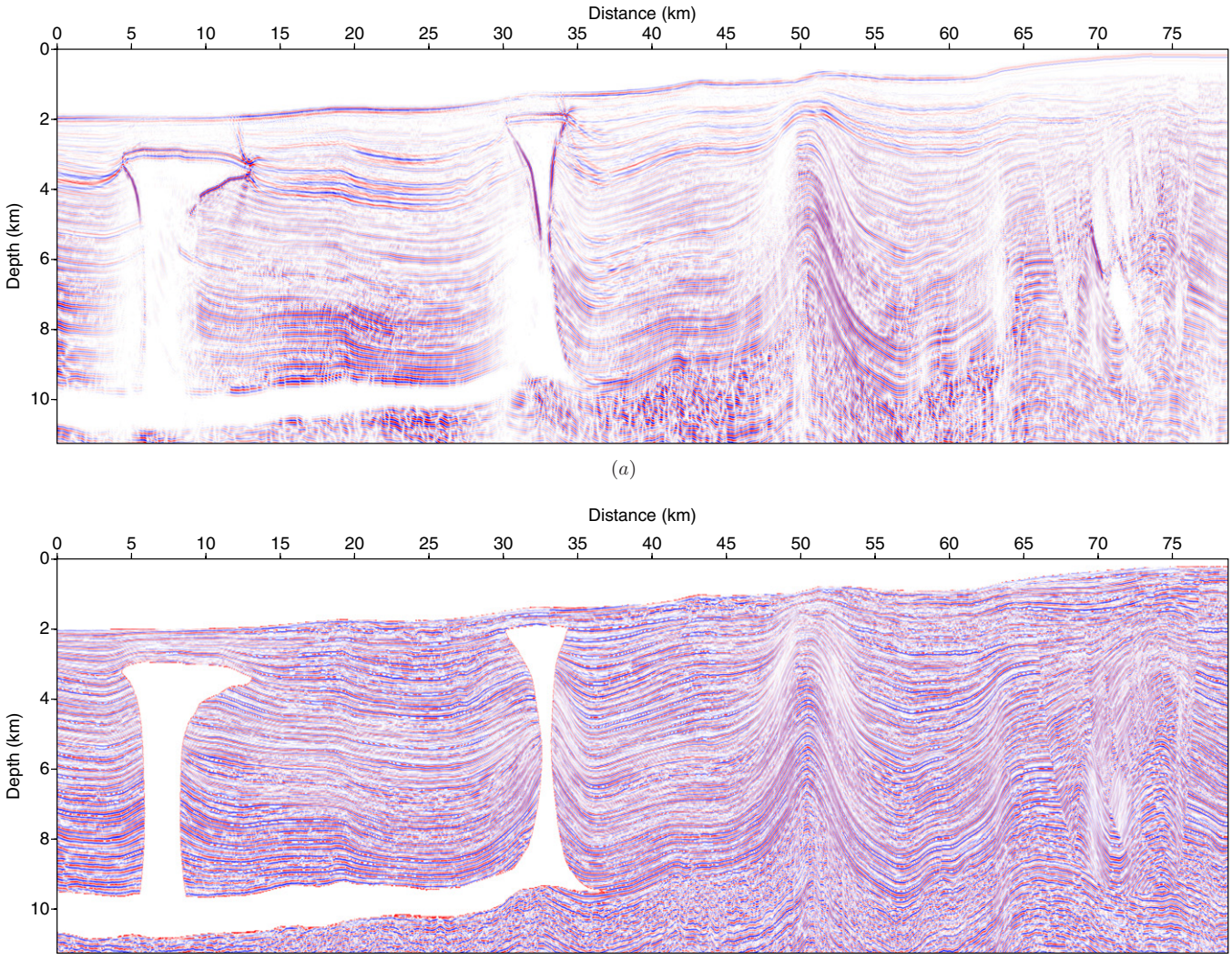

Figure 4. TTI RTM image of the BP 2D TTI model in (*a*) is compared with the actual reflectivity model in (*b*).

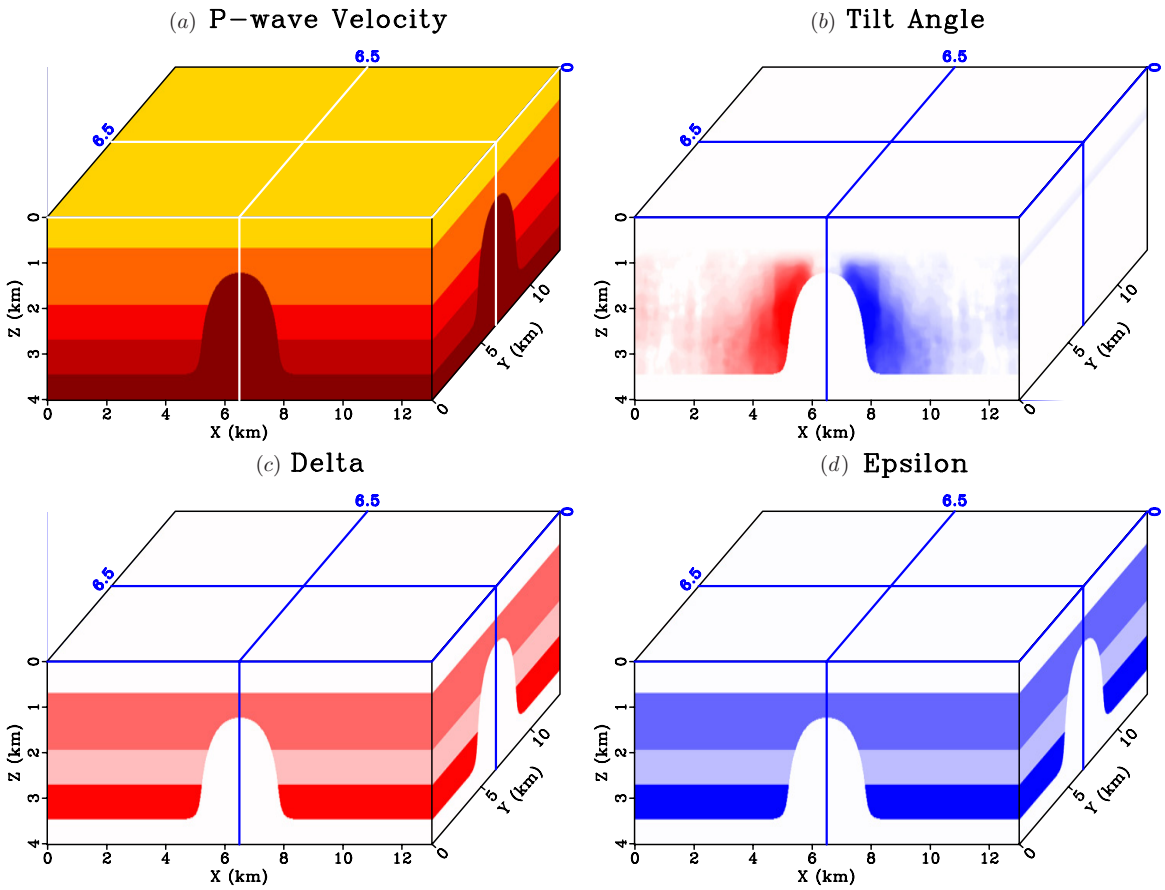

Figure 5. 3D salt dome models: (*a*) v_v and (*b*) θ; (*c*) and (*d*) are Thomsen's parameters δ and ε. The front frame and side frame correspond to 2D slices at $Y = 6.5$ km and $X = 6.5$ km, respectively.

Table 3. 2D 1-shot RTM runtime comparison using different schemes.

	Method 2D runtime (min)		
Media	FD	PS	Hybrid
Isotropic	1.9	16.4	–
VTI	9.2	28.0	–
TTI	68.7	94.4	65.5

standard isotropic RTM, conventional VTI coupled equations (equations (5*a*) and (5*b*) of Du *et al* (2008)) and TTI coupled equations (equations (2) and (3) of Fletcher *et al* (2009)) using the FD scheme are also implemented and compared.

4.1. 2D example

The grid size of the computational 2D domain is 1001 grid points in Z and 1061 grid points in X, and a total number of 12 267 time steps is computed for both forward propagation and back propagation in migrating a CSG. The computational costs for different RTM strategies running on a 12-core Intel Xeon computing node are listed in table 3, and the corresponding histogram is displayed in figure 3.

From the runtime comparison, we see that a transfer from isotropy to anisotropy complicates the RTM algorithm by taking into account two or more anisotropic parameters, which results in gradually increasing computational costs with increasing anisotropic complexities. We also note that the standard PS method costs much more than the conventional FD approach due to the introduced FFTs for better accuracy. However, by solving the TTI pure P-wave equation in a hybrid method, the RTM cost per shot (24 534 time steps in total) is reduced from 94.4 to 65.5 min with the PS method, where a saving of 31% in computational cost is achieved. And it is even less expensive than the FD solution for the TTI coupled equations (68.7 min per shot), which usually suffers from shear-wave artefacts.

A stacked TTI RTM image of all 1641 CSGs using the hybrid solution to the pure P-wave equation is shown in figure 4(*a*). It is almost a perfect replication of the actual reflectivity model as shown in figure 4(*b*) except for some white shadows due to imperfect illuminations.

4.2. 3D example

The 2D example shown above demonstrated the efficiency of the hybrid strategy. To further examine the performance of the hybrid scheme, we test it on a 3D TTI salt dome model.

The models shown in figure 5 contain five major layers: a water layer, three sedimentary layers with a salt dome embedded in the middle and the salt base. The water layer ($v_v = 1.5\,\mathrm{km\,s^{-1}}$) and the salt ($v_v = 4.5\,\mathrm{km\,s^{-1}}$) are set to be isotropic ($\delta = \varepsilon = 0$, $\theta = 0^\circ$). The three sedimentary layers are TTI media with

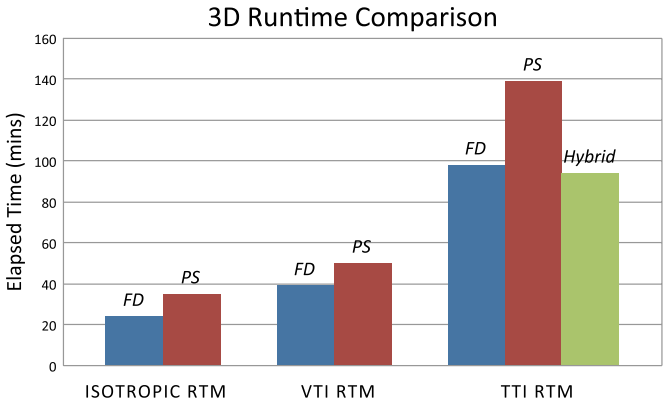

Figure 6. Histogram comparison of the 3D RTM runtimes.

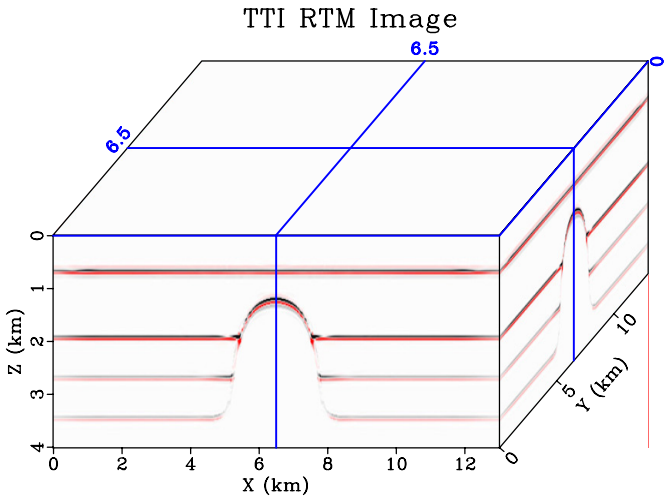

Figure 7. TTI RTM image of the 3D salt dome model.

Table 4. 3D 1-shot RTM runtime comparison using different schemes.

	Method 3D runtime (min)		
Media	FD	PS	Hybrid
Isotropic	23.7	35.4	–
VTI	39.2	50.1	–
TTI	98.2	138.5	94.3

$v_v = 2.5, 3.5, 4.0\,\mathrm{km\,s^{-1}}$ (figure 5(*a*)); $\delta = 0.06, 0.025, 0.1$ (figure 5(*c*)) and $\varepsilon = 0.12, 0.05, 0.2$ (figure 5(*d*)) from shallow to deep. A simple 2.5D tilt angle model (range from -50° to 50°) was adopted with a tilt axis normal to the salt flank (figure 5(*b*)). A constant $\phi = 15^\circ$ is used in this case.

The 3D model has 201 grid points along Z and 651 grid points along X and Y with a uniform grid point spacing of 20 m in all three directions. For each CSG, the 3D RTM used a local computation grid of $301 \times 401 \times 401$ (100 grid points padding in each direction) with a total of 4802 time steps in both the forward and backward propagation operations. Table 4 lists the runtimes of the 3D TTI RTM using one CSG on the 12-core computing node. The isotropic and VTI RTM runtime results are also presented for comparison. These computational costs with different RTM algorithms are then graphically illustrated in figure 6.

For the 3D model, the hybrid method is still faster than the PS method by around 29%, because more than half the 3D FFTs are replaced by less expensive FD calculations. Besides, as we saw in the 2D case, the hybrid scheme in 3D achieves an even better computational efficiency in comparison with the standard FD solution to the TTI coupled equations. Figure 7 displays the TTI RTM image of this 3D salt dome model.

5. Conclusions

We have rewritten the TTI pure P-wave equation in a form which reduces the number of FFTs per time step simulation. Also, a hybrid pseudospectral (PS)/finite-difference (FD) scheme is proposed to solve this equation, where wavenumber operators are replaced by inexpensive FD spatial operators. The computational costs of TTI RTM with the hybrid method are reduced by 31% for the 2D case and 29% for the 3D case. Therefore, the hybrid PS/FD scheme makes the TTI pure P-wave equation more practical and realistic for industrial-scale 3D migration problems.

Acknowledgments

We thank the Supercomputing Laboratory at King Abdullah University of Science and Technology (KAUST) in Thuwal, Saudi Arabia, for the computer cycles provided to this project. We would also like to thank BP for making the 2D TTI model and data set available. We acknowledge the anonymous reviewers for their valuable comments and suggestions.

References

Alkhalifah T 1998 Acoustic approximations for processing in transversely isotropic media *Geophysics* **63** 623–31

Alkhalifah T 2000 An acoustic wave equation for anisotropic media *Geophysics* **65** 1239–50

Bos L and Slawinski M A 2010 Elastodynamic equations: characteristics, wavefronts and rays *Q. J. Mech. Appl. Math.* **63** 23–38

Chu C, Macy B K and Anno P D 2011 Approximation of pure acoustic seismic wave propagation in TTI media *Geophysics* **76** WB97–107

Crawley S, Brandsberg-Dahl S, McClean J and Chemingui N 2010 TTI reverse time migration using the pseudo-analytic method *Leading Edge* **29** 1378–84

Du X, Fletcher R and Fowler P J 2008 A new pseudo-acoustic wave equation for VTI media *70th Annu. Conf. and Exhibition (EAGE Extended Abstracts)* p H033 (available at http://earthdoc.eage.org/publication/publicationdetails/?publication=9934)

Duveneck E and Bakker P M 2011 Stable p-wave modeling for reverse-time migration in tilted TI media *Geophysics* **76** S65–75

Epstein M, Peter D and Slawinski M A 2012 Combining ray-tracing techniques and finite-element modelling in deformable media *Q. J. Mech. Appl. Math.* **65** 87–112

Etgen J T and Brandsberg-Dahl S 2009 The pseudo-analytical method: application of pseudo-Laplacians to acoustic and acoustic anisotropic wave propagation *SEG Technical Program Expanded Abstracts* vol 28 pp 2552–6

Fletcher R, Du X and Fowler P J 2009 Reverse time migration in tilted transversely isotropic (TTI) media *Geophysics* **74** WCA179–87

Fowler P J, Du X and Fletcher R P 2010 Coupled equations for reverse time migration in transversely isotropic media *Geophysics* **75** S11–22

Harlan W 1995 Flexible seismic traveltime tomography applied to diving waves *Stanford Exploration Project Report* 89 pp 145–64 (available at http://sepwww.stanford.edu/public/docs/sep89/harlan/paper_html)

Kosloff D D and Baysal E 1982 Forward modeling by a Fourier method *Geophysics* **47** 1402–12

Liu F, Morton S A, Jiang S, Lideng N and Leveille J P 2009 Decoupled wave equations for P and SV waves in an acoustic VTI media *SEG Technical Program Expanded Abstracts* vol 28 pp 2844–8 (available at http://library.seg.org/doi/abs/10.1190/1.3255440)

Pestana R C, Ursin B and Stoffa P L 2012 Rapid expansion and pseudo spectral implementation for reverse time migration in VTI media *J. Geophys. Eng.* **9** 291

Reshef M, Kosloff D, Edwards M and Hsiung C 1988 Three dimensional acoustic modeling by the Fourier method *Geophysics* **53** 1175–83

Thomsen L 1986 Weak elastic anisotropy *Geophysics* **51** 1954–66

Zhan G, Pestana R C and Stoffa P L 2012 Decoupled equations for reverse time migration in tilted transversely isotropic media *Geophysics* **77** T37–45

Zhou H, Zhang G and Bloor R 2006a An anisotropic acoustic wave equation for VTI media *68th Annu. Conf. and Exhibition (EAGE Extended Abstracts)* p H033 (available at http://earthdoc.eage.org/publication/publicationdetails/?publication=398)

Zhou H, Zhang G and Bloor R 2006b An anisotropic acoustic wave equation for modeling and migration in 2D TTI media *SEG Technical Program Expanded Abstracts* vol 25 pp 194–8 (available at http://library.seg.org/doi/abs/10.1190/1.2369913)